ISSN 1054-660X, Laser Physics, 2011, Vol. 21, No. 1, pp. 130–136.

Brownian Diffusion of Gold Nanoparticles in an Optical Trap Studied by Fluorescence Correlation Spectroscopy[1]

J. Wang[a], Z. Li[a], C. P. Yao[a], F. Xue[a], Z. X. Zhang[a, *], and G. Hüttmann[b]

[a] *The Key Laboratory of Biomedical Information Engineering of Ministry of Education, School of Lifescience and Technology, Xi'an Jiaotong University, 710049 Xi'an, China*

[b] *Institut für Biomedizinische Optik, Universität zu Lübeck, Peter-Monnik Weg 4, 23562, Lübeck, Germany*

*e-mail: zxzhang@mail.xjtu.edu.cn

Received August 10, 2010; in final form, August 14, 2010; published online December 4, 2010

Abstract—The effect of thermal-induced Brownian motion on gold nanoparticles (Au NPs) in optical traps is studied by fluorescence correlation spectroscopy (FCS) method. The Brownian motion and optical trapping potential are investigated by the decay time of the FCS curve and the laser power. It is shown that that the probability of finding a gold nanoparticle in the trap depends on the ratio of the optical energy of the particle to its thermal energy. A power threshold is observed by the decay time as a function of laser power. The experimental studies show that the temperature rise does not seriously affect the average number of particles in the focal spot, but the average residence time is more sensitively affected by the temperature.

DOI: 10.1134/S1054660X1101021X

1. INTRODUCTION

Gold nanoparticles (Au NPs) have found broad applications in nanomaterials and nanobiotechnology [1, 2]. Au NPs have found use, for example, as local heat sources causing plasma membrane permeability [3–5], as photoluminescience resources with their well-defined plasmon resonances [6–9], and in optical trapping studies, gold nanoparticles have been investigated as superior handles relative to polystyrene (PS) beads because gold's high polarizability could lead to higher trap efficiency [10]. Further more, when the particle size is smaller than the size of the trapping laser beam, a number of Au NPs can also be trapped and an assembly is formed at the focal spot. It was observed that Au NPs were trapped one by one at the focal spot [11].

With an increase in the application of optical tweezers, much more tiny particles such as metal nanoparticles have become the targets of the manipulation [12, 13]. As an approach to the enhancement of radiation force to attain the manipulation of smaller nanoparticles, resonance effects, in addition to nonresonant conventional optical manipulation, have been also studied.

Because at the location of maximum gradient of the intensity of a laser beam, the gradient force of Au NPs is stronger than the scattering force which results from the radiation pressure that tends to push an object along a beam's propagation direction. In this paper, we observed the diffusion speed of Au NPs was slow down by pulse laser beam, with the diffusion forces arise from the Brownian motion. For a comprehensive analysis of the optical gradient force acting on molecules, fluorescence correlation spectroscopy (FCS) is a promising tool. We try to examine radiation force with Brownian motion on Au NPs in the focal spot by means of FCS.

FCS is a powerful tool to study Brownian motion of single fluorescent molecules in solution, since its introduction more than 30 years ago [14, 15]. FCS is based on statistical analysis of the temporal behavior of spontaneous fluorescence intensity. In practice, the method requires to detect the signal from a few molecules diffusing through in a very small detection volume. The number of fluorescent molecules and the diffusion coefficient are obtained from the autocorrelation function of the fluorescence intensity. Now FCS has become one of the significant techniques for measuring molecular diffusion dynamics and concentration in small spaces [16]. Recently, combinations of the time-correlated single-photon correlation (TCSPC) and FCS have been proposed, for improving signal-to-noise ratio of an FCS measurement by time-gating photons on the nanosecond timescale [17–19]. However, only handful studies of applications of FCS have been reported to elucidation of optical trapping kinetics. Hosokawa et al. reported that polymer nanoparticles with 24–200 nm diameters were assembled by radiation force in the potential well [16]. Ito et al. using a computing method based on Brownian dynamics simulation to investigate the optical potential with the temperature elevation under optical trapping condition [13].

In this paper, we fit the FCS curve and the decay times of the curve are observed as a function of the laser power and diameter of Au NPs. In FCS, the decay time τ_D is the characteristic diffusion time during which a molecule resides in the observation vol-

[1] The article is published in the original.

ume [20], and in this case is the average lifetime an Au NPs captured by optical trap. It is clearly found that at the focal spot of pulse laser beam the Brownian motion of Au NPs induced by photon thermal effect is stronger than the gradient force below a threshold. With the increasing of the laser power, gradient force increases more than the former one and upper the threshold the decay times of the FCS curve are increasing with the laser power. The experimental results are compared with a numerical simulation based on Monte Carlo method for quantitative evaluation of mechanical interaction between optical force potential and temperature elevation.

2. EXPERIMENT SETUP AND SIMULATION METHODS

The FCS experiments were performed by a TCSPC module connected to a two-photon microscope. Our experimental setup routinely uses the compact solid-state, mode-locked 80 MHz titanium: sapphire laser (MaiTai, Spectra Physics, Darmstadt, Germany) with a tuning range of 710 to 920 nm, a mean output power of 900 mW at 800 nm, and a laser pulse width of 75 fs. The scanning module contains a motorized a shutter, beam attenuator, and a two axis galvoscanner. The fluorescent signal was detected by a photomultiplier (H7732-01, Hamamatsu, Herrsching, Germany) after passing a beam splitter and a short-pass filter (BG39, Scott, Mainz, Germany). The beam is focused to a diffraction-limited spot by a ×40 objective (Plan Neofluar NA. 1.30, Zeiss, Goettingen, Germany, mean working distance: 140 mm) onto the sample. The signals were recorded by the TCSPC board (SPC-830, Becker and Hickl, Berlin, Germany). The TCSPC device is configured as a large first-in-first-out (FIFO) buffer then a time-tag recording is taken. The output of the FIFO is continuously read by the computer. Consequently, the time-tag mode delivers a continuous and virtually unlimited stream of photon data [10].

The decay time of the different size Au NPs (British Biocell International, 15, 30, and 50 nm sized) at a concentration of ~10^{10} particles/ml (5–30 pM) were measured using FCS. Fluorescence intensity was acquired by the PMT in 4 min for the power lower than 100 mW and 2 min for the power upper than 100 mW. The autocorrelation function was determined for ten separate runs. All experiments were performed at room temperature.

We use Dye-doped polystyrene latex nanoparticles (Molecular Probes, FluoSpheres, carboxylate-modified orange, diameters 100 nm) as calibration of the FCS setup. These beads deliver a bright fluorescence signal and a well-defined slowly decaying autocorrelation curve due to their slow diffusion. The latex beads were diluted with distilled water to a concentration of ~10^{11} particles/ml. The two-photon excitation wavelength we used was 750 nm with the power 20–50 mW. The FCS curve is represented as [20]

$$G(\tau) = \frac{1}{\langle N\rangle(1+\tau/\tau_D)(1+\tau/(S^2\tau_D))^{1/2}} + 1, \quad (1)$$

where N is the average number of particles in the laser spot and $S = z_0/\omega_0$ is the ratio of the axial to radial dimensions of the laser spot with the laser beam waist ω_0 in the focal plane and z_0 on the optical axis. τ_D is the decay time that corresponds to the average transit time of nanoparticles in the focal spot of laser beam and is obtained by the analytical fitting of the FCS curves to Eq. (1). The decay time of the latex beads we got was 13.2 ± 2.5 ms, almost the same to the results of Hosokawa's [21]. The diffusion coefficient D is calculated to be 4.4 μm^2/s [19] using the Stokes–Einstein equation $D = K_B T/6\pi\eta r$, where η is viscosity of the solution, T is the absolute temperature and assumed to be 293 K, K_B is Boltzmann's constant, and r is the radius of the particle. Then ω_0 is experimentally calculated to be 0.67 μm with the equation $D = w_0^2/8\tau_D$ and we estimated S^2 to be ~8.

Computational simulation is a powerful tool to reproduce molecular dynamics driven by the fluctuation in condensed phase; comparing experimental results with simulated ones can elucidate complex and stochastic phenomena [13, 22, 23]. For this purpose, a Monte Carlo simulation has been presented for the rational interpretation of experimental results of FCS.

The simulation of an FCS measurement was conducted in three stages: (a) generation of molecular trajectories, (b) generation of detected fluorescence time course, $F(t)$, on the basis of the molecular trajectories, and (c) computation of $G(\tau)$ from $F(t)$. A system of molecules evolving by Brownian dynamics is described by the following algebraic equation:

$$r(t+h) = r(t) + \frac{1}{\xi}hf(t) + \Delta r^B \quad (\xi = 6\pi\eta a). \quad (2)$$

Here, t is the initial time, $r(t + h)$ is the coordinate of molecule after a short time step h from the time origin, $f(t)$ is the external force acting on the molecule at the time origin, ξ is the viscous drag, η is the viscosity of the liquid, and a is the radius of the molecule, and Δr^B is the randomed displacement of Brownian motion. Δr^B is a Gaussian-distributed random number with average zero and standard deviation $\frac{2k_B Th}{\xi}$, where k_B is the Boltzmann constant and T is the Kelvin temperature.

In our study, the random movement of a molecule was calculated in such a manner that the long-time statistical distribution of the random walk obeys the distribution function. The molecule randomly moves step by step and sometimes stays in the sampling area

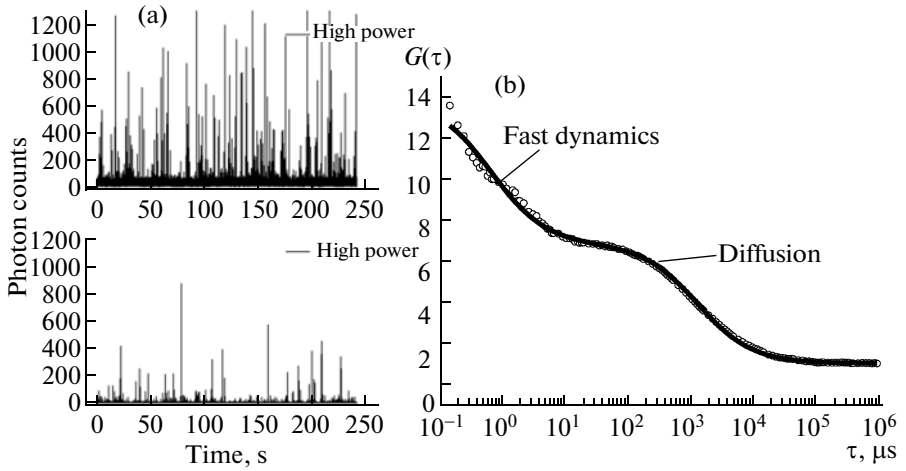

Fig. 1. (a) Temporal profile of two-photon excitation fluorescence intensity of 30-nm-sized Au NPs suspensions. At low powers (20 mW), bursts occurred unbiased and represented true local concentration of nanoparticles; at high powers (150 mW), the apparent local concentration of particles increased as evinced by more frequent bursts. (b) Typical autocorrelation curve of the fluorescence emitted from 30 nm-sized Au NPs suspensions. Solid line is the result of fitting of Eq. (2). The plots at the early time are due to a transient bleaching of Au NPs.

of a confocal microscope. For a three-dimensional Gaussion the excitation light intensity at position r_i is

$$I_{\mathrm{exc}}(r_i, z_i) = I(0)\exp\left[-\left(\frac{(x_i-x_0)^2+(y_i-y_0)^2+((z_i-z_0)/S)^2}{2\omega_0^2}\right)\right], \quad (3)$$

where $S = z_0/\omega_0$ is the ratio of the axial to radial dimensions of the laser spot with the laser beam waist ω_0 in the focal plane and z_0 on the optical axis. At the same time we consider the gradient force acting on molecules in the optical force potential. The trapping potential can be calculated by [24]

$$u(z) = u_0\exp\left(\frac{2\pi\alpha n}{ck_{\mathrm{B}}T}I(0)\exp(-z/\delta)\right). \quad (4)$$

This gives the steady state density of particles in the light field as a function of position. u_0 is the background density and the transmitted intensity decays in proportion to

$$I(z) = I(0)\exp(-z/\delta), \quad (5)$$

where the decay length

$$\delta = \frac{\lambda}{4\pi\sqrt{\varepsilon_i\sin^2\theta_i-\varepsilon_t}} \quad (6)$$

depends on the relative permittivities of the incident medium ε_i and the transmitting medium ε_t, for light incident at angle θ_i to the surface normal. The effective polarizability α of the spherical particle in the supporting medium is $\sim a^3$, where a is the radius of the molecule. It rapidly approaches the background value $z > \delta$ for depending on the strength of the trap which depends on the intensity of the light. If the $u(z)/u_0 > 1$, it means the effect of the optical trap is stronger than the Brownian motion and the particles are gathered at the focal spot. Then we use

$$G(\tau) = \frac{\langle\delta F(t)\delta F(t+\tau)\rangle}{\langle F(t)\rangle^2} \quad (7)$$

to calculate $G(\tau)$ from $F(t)$.

We consider the interface to be between glass and water, the laser beam waist to be 0.67 μm, and the refractive index of Au NPs to be varied from 1.33 to 1.55 [1], and the trajectory of 200 molecules, whose initial positions were chosen at random, was computed in a $10 \times 10 \times 10$ μm^3 box with the time step h setting to 200 ns. The system was typically equilibrated by a run of 3 s.

3. RESULTS AND DISCUSSION

In generally, the plasmon resonance-based optical trapping method with a cw laser is used to achieve stable trapping of Au NPs of different shapes and composition [10]. When use a pulse laser for probing, since the free Brownian motion of the Au NPs is affected by the weak trapping potential, the Au NPs should also stay in the focal spot for a longer time than other places. We can use FCS method to study this complex Brownian motion.

As Geddes et al. have observed, Au NPs showed a time-dependent increase in emission upon illumination from point-like locations and the emission displayed blinking [25]. This may be caused by the transient vapor bubbles around AuNPs [26, 27]. The generation of a bubble around an AuNP may explain the discovered effect of optical amplification: the surface

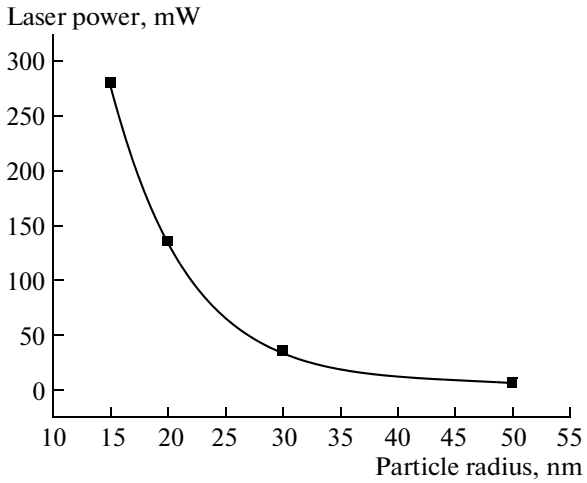

Fig. 2. The threshold for trapping Au NPs as a function of laser power, simulation results.

of the bubble increases the gradient of the refractive index around an AuNP, and moreover an expanding bubble increases the diameter of the scattering object, thus additionally increasing the optical scattering. The detected transient change in the optical contrast is quite dramatic due to the bleaching of the scattering around one AuNP and the amplification the scattering around the other AuNP [27].

When chemical kinetics occur on a time scale much faster than the decay time τ_D, the dynamics of the m independent transition pathways between a fluorescent state and dark state(s) can be described by [20]

$$G(\tau) = G_D(\tau)\prod_{i=1}^{m}\frac{(1-f_i+f_i e^{-\tau/\tau_i})}{(1-f_i)}. \qquad (8)$$

The fraction f_i of molecules residing in a dark state for a characteristic time τ_i can be determined from the measurements; for diffusion alone, $f_i = 0$ and $G(\tau) = G_D(\tau)$. At the early time, we can use Eq. (8) to take into account the fact that a fraction f_1 of the fluorophores is in transient bleaching or amplification the scattering state with an average half-life time τ_1. In this study, we adopted Eq. (8) with $i = 1$ as a simple form because our focus is the diffusion of the particles. As Fig. 1 shows, the autocorrelation curve of the fluorescence can be fitted quite well except at the early time. The spikelike signal in Fig. 1a is due to fluorescence from a trapped particle which escapes from the well at shorts times.

A nanoparticle at the focal spot of the laser beam will be heating by the photon thermal energy. According to the Stokes–Einstein equation, the diffusion coefficient of the particles will be increasing with the increasing of the temperature. On the other hand, the gradient force of a particle in the optical trap is associated with the energy required to polarize a particle in

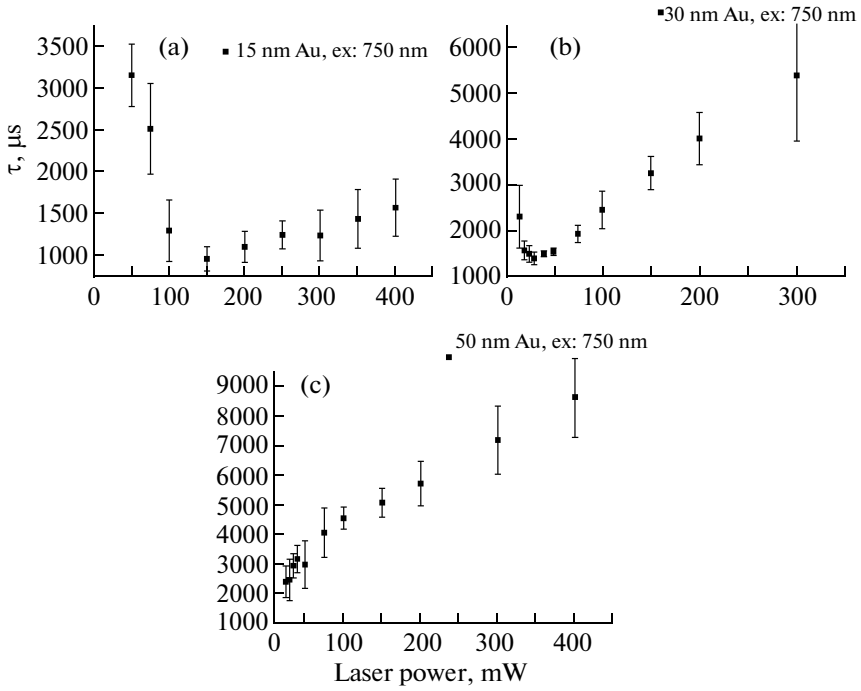

Fig. 3. The decay time of the FCS curves as a function of laser power. The excitation wavelength we used was 750 nm. (a) 15 nm-sized Au NPs. It is clearly observed that if the power is less than 150 mW the Brownian motion of the particles is stronger than the trapping potential. (b) 30 nm-sized Au NPs. (c) 50 nm-sized Au NPs.

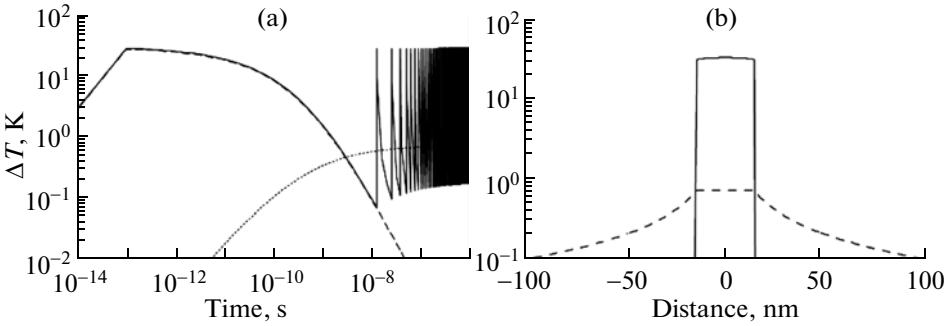

Fig. 4. Calculation of the temperature in and around single gold particles during laser irradiation. (a) Temperature course during the irradiation with 1 mW radiant flux focused to a spot of 700 nm (solid black line). Rectangular pulses with 100 fs width and 12 nm temporal separation were assumed. Additionally the temperature course after one pulse (dashed line) and after true CW irradiation with the same average radiant flux (dotted line). (b) Spatial temperature distribution at the end of the first pulse (solid line) and after 10 μs irradiation (dashed line).

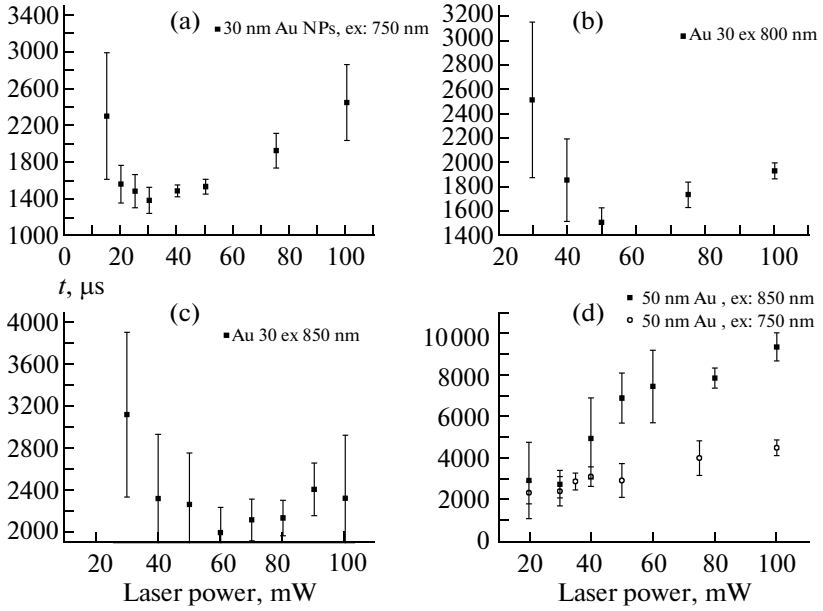

Fig. 5. Laser power dependence of the FCS decay time with different excitation wavelength. (a) 30 nm-sized Au NPs with excitation wavelength 750 nm. (b) 30 nm-sized Au NPs with 800 nm. (c) 30 nm-sized Au NPs with 850 nm. (d) 50 nm Au NPs, open circles are decay time with excitation wavelength 750 nm, close squares are with 850 nm.

an electric field. If the trapping potential is stronger than the Brownian motion, the diffusion speed of the particles should be decreasing with the increasing of the laser power. Then we can use the decay time of the FCS curve to study this, in this case it is the average lifetime an AuNP captured by optical trap. As Fig. 2 shows, these two parts can be clearly separate by an energy threshold. Below the threshold, the diffusion speed of the Au NPs is increased by the laser power, that means the Brownian motion of the particles is stronger than the optical force. Upon the threshold, the trapping potential is stronger than the Brownian motion.

At the room temperature, the threshold for trapping 50nm-sized Au NPs would be 6 mW, a 35 mW laser would trap 30 nm-sized Au NPs and a 280 mW laser would trap 15 nm-sized Au NPs in the simulation, as Fig. 2 shows. But in the experimental results, as Fig. 3 shows, the threshold for trapping 15 nm-sized Au NPs is 150 mW, for 30 nm-sized Au NPs is 30 mW and for 50 nm-sized Au NPs is less than 15 mW. The results of 15 nm-sized are quiet different from that we calculate, because of the significant heating induced by optical trap. Perkins et al. have found dramatic heating of 266°C per 1 W (laser power) at the most common trapping wavelength (1064 nm) [28]. We have calculated the temperature in and around single

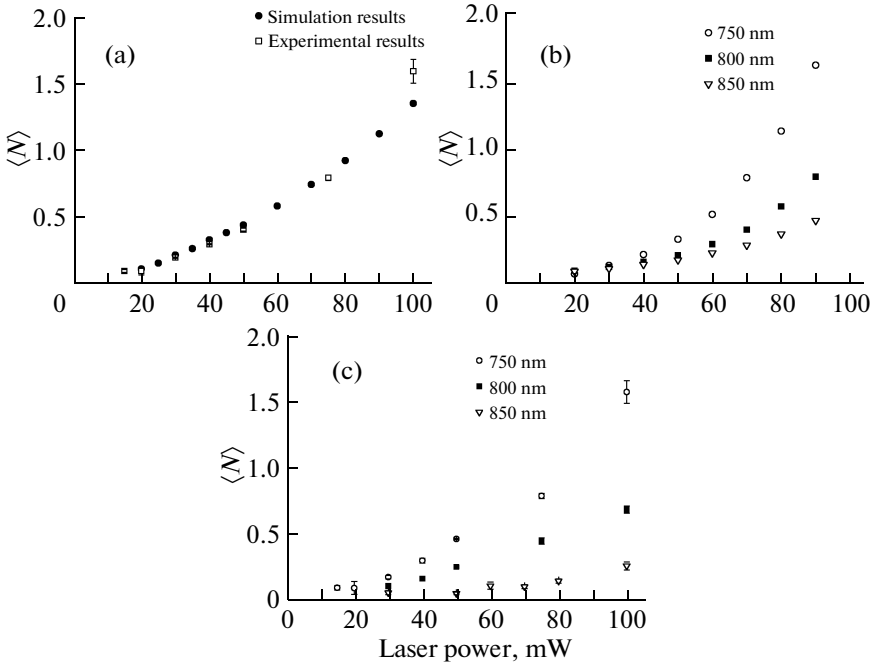

Fig. 6. Laser power dependence of the average number of molecules, N, with different excitation wavelength. (a) 30 nm-sized Au NPs with excitation wavelength 750 nm, close circles are simulation results and open squares are experimental results. (b) Simulation results of the average number of 30 nm-sized Au NPs with 750 (open circles), 800 (close squares), and 850 nm (open triangles). (c) Experimental results of the average number of 30 nm-sized Au NPs with 750 (open circles), 800 (close squares), and 850 nm (open triangles).

Au NPs during laser irradiation, as Fig. 4 shows. The temperatures inside and in the surrounding of the particles were calculated by an analytical solution of the differential equation of heat diffusion for a single spherical particle which has different thermal properties than the surrounding medium. A series of rectangular 100 fs broad laser pulses with 80 MHz repetition rate was assumed. Individual particle absorption was calculated form data which were provided by the manufacturer of the particles for a wavelength of 520 nm (absorption of 5 cm^{-1} at a particle concentration of 7.8×10^{11} ml^{-1}). By absorption measurements with a scanning photometer (Lambda 14, Perkin Elmer, Überlingen, Germany) the absorption cross-section of 5% of the geometrical cross-section resulted for 30 nm particles. The focal diameter of the 1.3 NA object was calculated by Abbe's formula to be 700 nm. The calculations for tightly focused irradiation with 80-MHz repetition rate reveal that the temperature is 6.8 times larger after a few microseconds than the temperature increase cause by a single pulse [29]. Theoretically the temperature of the 15 nm-sized Au NPs induced by laser may be as high as 450 K. Water's viscosity also decreases as temperature increases. The trap stiffness (k_{trap}) depends linearly on temperature ($k_{trap} = k_B T/\langle x^2 \rangle$, where x is the bead's position) [28]. Then the trap stiffness may be 50% higher than we simulate using Eq. (4).

Below the threshold, the decay time is expressed as

$$\tau_D = \omega^2/8D = 6\pi\eta r\omega^2/8K_B T \qquad (9)$$

and ΔT is liner to the laser power [28]. As Fig. 5 shows, the decay time of 30 nm-sized Au NPs changes faster than 15 nm-sized Au NPs. We fitted the FCS curve using Eq. (9), and the factor to r of 15 nm-sized particles we got was 6.96E-6, of 30 nm-sized particles was 1.32E-5, same to the radio of radius. Upon the threshold, the trapping potential $|U_{trap}|$ is presented as [16]

$$|U_{trap}| = 2\alpha P n_2/(\pi c \varepsilon_2 \omega_0^2), \qquad (10)$$

where α is the polarizability of the nanoparticle and $\sim a^3$, where a is the radius of the particles, P is the laser power, c is the speed of the light, and n_2 and ε_2 are the refractive index and dielectric constant of water. According to Eq. (10) we can assume that decay time is liner to the laser power P and a^3, as we see from Fig. 3. The slope of 15 nm-sized Au NPs upon the threshold is 2.36, the slope of 30 nm-sized Au NPs is 10.30. The slope of 50 nm-sized Au NPs is 13.70 and the slope of 50 nm-sized beads between 20–100 mW is 34.94.

According to Eq. (6), the threshold is also influenced by the excitation wavelength λ. We can see the threshold increases with the λ increasing, as Fig. 5 shows. The threshold for 30 nm-sized Au NPs with 750 nm is 30 mW and that for 850 nm is 60 mW. We

can't observed the threshold of 50 nm-sized Au NPs with 750 nm in the experiments, but the threshold with 850 nm may be 30 mW. This means it need larger laser power to trap an Au Np when using longer wavelength.

At the same time, the average number of Au NPs, N, is also well studied. The value of N increases with an increase in the trapping potential. Both simulation results and experimental results suggest that the temperature rise does not seriously affect the average number of particles. Experimental results also show that the value of N increases faster under short wavelength than longer wavelength, as Fig. 6 shows.

4. CONCLUSIONS

The effect of thermal energy on the trapping of gold nanoparticles has been analyzed using a FCS method. The decay times of the FCS curves are observed as a function of the laser power and diameter of Au NPs. It is clearly that there is a laser power threshold that below the threshold the Brownian motion of the particles is stronger than the optical trapping potential, and upon the threshold the gradient force increases more than the Brownian motion. Below the threshold the decay time shows a liner factor to a, where a is the radius of particles and $1/T$, where T is the temperature. This may be useful in the photothermal therapy [30, 31]. Upon the threshold decay time is liner to the laser power P and a^3. The threshold is also influenced by the excitation wavelength. With longer wavelength, the power threshold is getting larger and upon the threshold the diffusion of the particles is slower. We assume that it is easier to trap molecule under short wavelength.

ACKNOWLEDGMENTS

This study was supported by the National Nature Science Foundation of China NSFC-60878056 and NSFC-60927011, and grant from the Ph. D. Programs Foundation of Ministry of Education of China no. 200806980024; Project Based Personel Exchange Programme with CSC and DAAD and the International Cooperation Key Project of Shaanxi Province 2009KW-15. We acknowledge Norbert Koop, Ramtin Rahmanzadeh, Barbara Flucke and Astrid Rodewald at institute of biomedical optics for their help during these experiments.

REFERENCES

1. M. C. Daniel and D. Astruc, Chem. Rev. **104**, 293 (2004).
2. V. K. Pustovalov and V. A. Babenko, Laser Phys. Lett. **1**, 516 (2004).
3. C. Yao, R. Rahmanzadeh, E. Endl, Z. Zhang, J. Gerdes, and G. Hüttmann, J. Biomed. Opt. **10**, 064012 (2005).
4. V. K. Pustovalov, Laser Phys. Lett. **2**, 401 (2005).
5. C. Yao, X. Qu, Z. Zhang, G. Hüttmann, and R. Rahmanzadeh, J. Biomed. Opt. **14**, 054034 (2009).
6. A. Lemelle, B. Veksler, I. S. Kozhevnikov, G. G. Akchurin, S. A. Piletsky, and I. Meglinski, Laser Phys. Lett. **6**, 71 (2009).
7. X. Qu, J. Wang, Z. Zhang, N. Koop, R. Rahmanzadeh, and G. Hüttmann, J. Biomed. Opt. **13**, 031217 (2008).
8. S. Tanev, V. V. Tuchin, and P. Paddon, Laser Phys. Lett. **3**, 594 (2006).
9. V. K. Pustovalov and V. A. Babenko, Laser Phys. Lett. **2**, 84 (2005).
10. P. M. Hansen, V. K. Bhatia, N. Harrit, and I. Oddershede, Nano Lett. **5**, 1937 (2005).
11. K. C. Toussaint, M. Liu, M. Pelton, J. Pesic, M. J. Guffey, P. Guyot-Sionnest, and N. F. Scherer, Opt. Express **15**, 12017 (2007).
12. T. Iida and H. Ishihara, Phys. Rev. Lett. **90**, 057403 (2003).
13. S. Ito, N. Toitani, H. Yamauchi, and H. Miyasaka, Phys. Rev. E **81**, 061402 (2010).
14. D. Magde, E. L. Elson, and W. W. Webb, Phys. Rev. Lett. **29**, 705 (1972).
15. D. Magde, E. L. Elson, and W. W. Webb, Biopolymers **13**, 29 (1974).
16. C. Hosokawa, H. Yoshikawa, and H. Masuhara, Phys. Rev. E **72**, 021408 (2005).
17. M. Wahl, I. Gregor, M. Patting, and J. Enderlein, Opt. Express **11**, 3583 (2003).
18. A. Benda, M. Hof, M. Wahl, M. Patting, R. Erdmann, and P. Kapusta, Rev. Sci. Instrum. **76**, 003106 (2005).
19. P. Kapusta, M. Wahl, A. Benda, M. Hof, and J. Enderlein, J. Fluoresc. **17**, 43 (2007).
20. S. T. Hess, S. Huang, A. A. Heikal, and W. W. Webb, Biochem. **41**, 697 (2002).
21. C. Hosokawa, H. Yoshikawa, and H. Masuhara, Jpn. J. Appl. Phys. **45**, 453 (2006).
22. J. A. Dix, E. F. Y. Hom, and A. S. Verkman, J. Phys. Chem. B **110**, 1896 (2006).
23. T. Wocjan, J. Krieger, O. Krichevsky, and J. Langowski, Phys. Chem. Chem. Phys. **11**, 10671 (2009).
24. T. J. Davis, Opt. Express **15**, 2702 (2007).
25. C. D. Geddes, A. Parfenov, I. Gryczynski, and J. R. Lakowicz, Chem. Phys. Lett. **380**, 269 (2003).
26. V. K. Pustovalov, A. S. Smetannikov, and V. P. Zharov, Laser Phys. Lett. **5**, 775 (2008).
27. E. Y. Lukianova-Hleb and D. O. Lapotko, Nano Lett. **9**, 2160 (2009).
28. Y. Seal, A. E. Carpenter, and T. T. Perkins, Opt. Lett. **31**, 2429 (2006).
29. A. Vogel, J. Noack, G. Hüttmann, and G. Paltauf, Appl. Phys. B **81**, 1015 (2005).
30. A. V. Kabashin, Laser Phys. **19**, 1136 (2009).
31. P. Pavlova, E. Borisova, L. Avramov, El. Petkova, and P. Troyanova, Laser Phys. **20**, 596 (2010).